Dysfunctional polycomb transcriptional repression contributes to Lamin A/C dependent muscular dystrophy
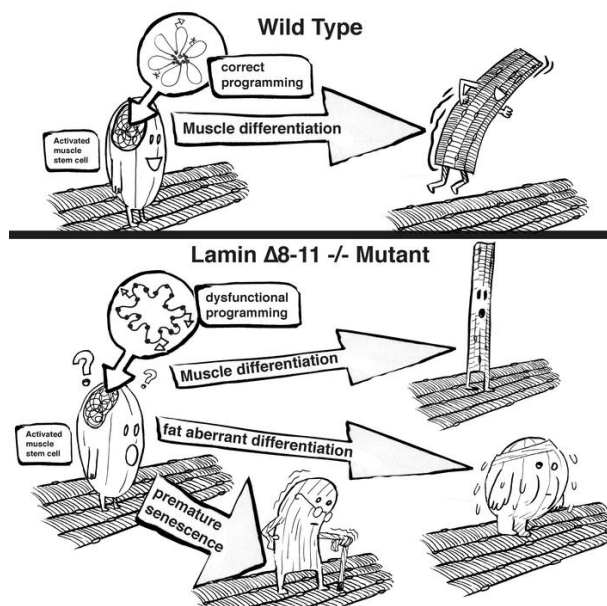
Andrea Bianchi, … , Claudia Bearzi, Chiara Lanzuolo

Research In-Press Preview **Muscle biology**

Graphical abstract

Dysfunctional Polycomb transcriptional repression contributes to Lamin A/C dependent muscular dystrophy

Andrea Bianchi[1, 2*], Chiara Mozzetta[2*§], Gloria Pegoli[3], Federica Lucini[1,3], Sara Valsoni[1,3, #], Valentina Rosti[4], Cristiano Petrini[5], Alice Cortesi[1], Francesco Gregoretti[6], Laura Antonelli[6], Gennaro Oliva[6], Marco De Bardi[3], Roberto Rizzi[1, 4], Beatrice Bodega[1], Diego Pasini[7], Francesco Ferrari[5, 8], Claudia Bearzi[1, 9] and Chiara Lanzuolo[3, 4]

1.   Istituto Nazionale di Genetica Molecolare "Romeo ed Enrica Invernizzi", Milan, Italy

2.   CNR Institute of Cellular Biology and Neurobiology, Rome, Italy

3.   IRCCS Santa Lucia Foundation, Rome, Italy

4.   CNR Institute of Biomedical Technologies, Milan, Italy

5.   IFOM, the FIRC Institute of Molecular Oncology, Milan, Italy

6.   CNR Institute for High Performance Computing and Networking, Naples, Italy

7.   European Institute of Oncology, Milan, Italy

8.   CNR Institute of Molecular Genetics "Luigi Luca Cavalli-Sforza", Pavia, Italy

9.   CNR Istituto di Biochimica e Biologia Cellulare, Rome, Italy

§.   Present address: CNR Institute of Molecular Biology and Pathology (IBPM), Rome, Italy

#.   Present address: San Raffaele Telethon Institute for Gene Therapy (SR-Tiget), IRCCS San Raffaele Scientific Institute, Milan, Italy

*   Equal contribution

Conflict of interest statement

The authors have declared that no conflict of interest exists.

Corresponding author: Lanzuolo Chiara. Via Fratelli Cervi, 93, 20090 Segrate (MI),

Italy; Phone: +39x 02 00660358; e-mail: chiara.lanzuolo@cnr.it

Running head

PcG dysfunctions in lamin dystrophy

Abstract

Lamin A is a component of the inner nuclear membrane that, together with epigenetic factors, organizes the genome in higher order structures required for transcriptional control. Mutations in the Lamin A/C gene cause several diseases, belonging to the class of laminopathies, including muscular dystrophies. Nevertheless, molecular mechanisms involved in the pathogenesis of Lamin A-dependent dystrophies are still largely unknown. Polycomb group of proteins (PcG) are epigenetic repressors and Lamin A interactors, primarily involved in the maintenance of cell identity. Using a murine model of Emery-Dreifuss Muscular Dystrophy (EDMD), we showed here that Lamin A loss deregulated PcG positioning in muscle satellite stem cells leading to de-repression of non-muscle specific genes and p16^{INK4a}, a senescence driver encoded in the *Cdkn2a* locus. This aberrant transcriptional programme caused impairment in self-renewal, loss of cell identity and premature exhaustion of quiescent satellite cell pool. Genetic ablation of *Cdkn2a* locus restored muscle stem cell properties in Lamin A/C null dystrophic mice. Our findings established a direct link between Lamin A and PcG epigenetic silencing and indicated that Lamin A-dependent muscular dystrophy can be ascribed to intrinsic epigenetic dysfunctions of muscle stem cells.

Introduction

The nuclear lamina (NL) is located in the inner part of the nuclear membrane and is made up of a complex network of type V filament proteins, the lamins (1, 2). In vertebrates lamin proteins are divided into A and B types, based on sequence homologies. A growing body of evidence suggests that lamins are directly involved in the functional control of the genome, by organizing its three dimensional positioning in the nuclear space, through the association with transcriptionally repressed large genomic regions, called Lamina-associated domains (LADs) (3). The crucial function of lamins is attested by an entire class of genetic diseases, called *laminopathies*, where specific components of the NL are altered (4). In particular, the study of Lamin A/C is gaining an increasing interest for three reasons: i) Lamin A/C plays an undisputed role in several cellular processes from mechanotransduction to cell differentiation; ii) Lamin A/C has a peculiar intranuclear distribution being present in the nucleoplasm as well as in the nuclear periphery (5); iii) Lamin A/C interacts with several epigenetic factors, exerting a functional control on transcriptional regulation (3, 6). One of the most studied Lamin A/C dependent cellular process is myogenesis because mutations in the *LMNA* gene lead to muscular dystrophies, as in the case of Emery Dreifuss Muscular Dystrophy (EDMD) (7). However, epigenetic mechanisms involved in lamin-dependent dystrophy are still largely unknown. PcG proteins are epigenetic repressors originally discovered for their central roles in development and cell differentiation (8) and recently described as functional partners of Lamin A/C (9-14). In the last years several evidence demonstrated that PcG proteins are involved in the regulation of adult stem cells (15, 16), safeguarding cell identity and preventing cell fate transition. In multipotent stem cells, PcG proteins ensure the correct balance between self-renewal and lineage-specific differentiation, promptly responding to the environmental changes. At the molecular level this is achieved through PcG binding at bivalent domains, genomic regions containing active and repressive epigenetic signatures and a poised RNA polymerase II (17). This epigenetic condition allows a

rapid transition from one transcriptional state to another, ensuring the correct expression of unique and specific cell lineage genes. Defects in these fine-tuned mechanisms lead to lack of cell identity (18) or pathological reprogramming (19).

Given their key role in regulating stem cells fate decisions and tissue homeostasis, it is conceivable that PcG dysfunctions contribute to lamin-dependent, tissue-specific human diseases. Here, we examined how the absence of Lamin A/C impacts muscle stem (satellite) cells (MuSCs) in vivo, and the role of PcG proteins in lamin muscular dystrophy. We found that MuSCs lacking Lamin A/C redistribute PcG-dependent histone marks leading to transcriptional upregulation of crucial PcG-target genes, such as non-muscle related genes. This leads to lack of MuSC cell identity and cellular senescence, determining a premature exhaustion of the muscular stem cell niche. Genetic ablation of the PcG-regulated *Cdkn2a* locus in lamin dystrophic mice restores MuSCs defects.

Results

Lamin A is required to preserve quiescent muscle stem cells (MuSC) pool.

We analysed the muscle stem cell niche composition in the severe dystrophic *Lmna* Δ8-11 -/- mice (homozygous, hom), together with their unaffected littermates, wild type (wt, *Lmna* Δ8-11 +/+) or heterozygous (het, *Lmna* Δ8-11 +/-), during dystrophy progression at 10, 14, 16 and 19 days after birth. In early stages of post-natal growth (d10 and d14) no differences were found in the relative amounts of quiescent (QSCs; PAX7+/MYOD-) and activated (ASCs; PAX7+/MYOD+) MuSCs (Figure 1A, 1B and S1A) among distinct genotypes. Conversely, starting from d16, an unbalance of MuSCs becomes evident in *Lmna* Δ8-11 -/- muscles, with a decreased proportion of QSCs compared to ASCs, mirroring a decline in myofibers cross sectional area (CSA) (Figure 1C). Of note, the overall amount of PAX7+ MuSCs was not significantly altered across the different genotypes (Figure S1B) and Ki67 staining at d19 confirmed that in *Lmna* Δ8-11 -/- muscles a lower amount of QSCs

5

(PAX7+/Ki67-) is present (Figure S1C). These findings suggested that *Lmna* Δ8-11 -/- MuSCs may be deficient in self-renewal capacity. To test this hypothesis, we isolated single myofibers at d19 and cultured them for 96h, monitoring their ability to give rise to self-renewing PAX7+/MYOD-, activated PAX7+/MYOD+ and differentiating PAX7-/MYOD+ cells (Figure 1D and 1E). In fibers isolated from *Lmna* Δ8-11 -/- muscles, we observed a decrease in the number of self-renewing PAX7+/MYOD- cells compared to wt, paralleled by a diminished number of differentiating cells (PAX7-/MYOD+) and an increased number of activated satellite cells. Immunostaining with the myogenic marker MYOG, involved in later stages of differentiation, highlighted a lower number of MYOG+/PAX7- cells in *Lmna* Δ8-11 -/- (Figure 1F and 1G) accompanied by proliferation defects ex vivo (Figure S1D). These findings suggest a defect in muscle differentiation, as described in (20), and a previously unreported self-renewal impairment. Interestingly, the healthy heterozygous *Lmna* Δ8-11 +/- mice, although not developing muscular dystrophy (21), presented an intermediate self-renewal phenotype between wt and homozygous *Lmna* Δ8-11 -/- (Figure 1D and 1E), suggesting that proper Lamin A levels are important for MuSCs homeostasis to preserve their self-renewal capacity. To further address this, we performed repeated muscle injuries on adult heterozygous *Lmna* Δ8-11 +/- mice, which show less Lamin A at mRNA and protein level (Figure S2A and S2B). Analysis of MuSC populations revealed a lower amount of QSCs in *Lmna* Δ8-11 +/- muscles upon repeated injuries (Figure 2A and 2B; Injured) and a decline in Pax7+ cells (Figure 2C; Injured), suggesting that Lamin A affects MuSCs self-renewal in a dose dependent manner.

Lmna Δ8-11 -/- dystrophic MuSCs display chromatin redistribution of PcG dependent signature

Our recent results showed a Lamin A/C-PcG crosstalk along in vitro myogenesis (10). We thus wondered if the altered MuSCs balance observed in *Lmna* Δ8-11 -/-

muscles might be ascribed to aberrant PcG functions. We first performed immunostaining of Ezh2, the catalytic subunit of Polycomb Repressive Complex 2 (PRC2) (Figure S3A) in d19 MuSCs. We fixed MuSCs before FACS-Sorting to preserve the nuclear architecture of Lamin A-deficient cells (see methods). We found a general intranuclear diffusion of Ezh2 in *Lmna* Δ8-11 -/- MuSCs, ascertained by measuring PcG bodies parameters (22) (Figure S3A, S3B and S3C). We also measured Ezh2 expression both in MuSCs and whole muscles (Figure S3D) and we analysed Ezh2 protein levels in whole muscles (Figure S3E and S3F). We found no major differences between Lmna Δ8-11 +/+ and -/- mice. To further analyse the Ezh2 intranuclear distribution in QSCs, we performed triple immunostaining on muscle cryosections (Figure S3G and S3H). Ezh2 levels, assessed measuring fluorescence intensity, were similar in Lmna Δ8-11 +/+ and -/- MuSCs both in PAX7+/Ki67- and PAX7+/Ki67+ cells. Since Ezh2 is hardly detectable in adult quiescent satellite cells (23-25), this result suggests that during post-natal growth developmental signals might instead contribute to maintain Ezh2 expression in non-proliferating MuSCs.

On the other hand, evaluation of the number of PcG bodies on the same sections highlighted a decrease in the number of Ezh2 bodies in the mutant (Figure S3I and S3J), leading us to conclude that the absence of Lamin A/C does not affect Ezh2 protein levels but influence its nuclear distribution. To gain further insights into possible PcG-dependent transcriptional defects, we performed RNA-sequencing on freshly isolated MuSCs at d19, finding 1424 upregulated genes and 1842 downregulated genes in the *Lmna* Δ8-11 -/- MuSCs as compared to the wt (Figure S4A). Interestingly, performing a Gene Set Enrichment Analysis (GSEA) based on differential expression generated after conditional ablation of Ezh2 in MuSCs (24) and *Lmna* Δ8-11 -/- up-regulated genes, we found a significant association between the two datasets suggesting that Lamin A absence impairs Ezh2 function (Figure

S4B). We also followed the deposition of the Ezh2 dependent H3K27me3 histone mark in *Lmna* Δ8-11 mice by quantitative spike-in ChIP-seq (26) (see additional methods, Figure S4C and S4D). Integrative analysis of RNA-seq and ChIP-seq revealed that up-regulated genes in Lmna Δ 8-11 -/- condition are significantly enriched for H3K27me3 targets (identified in wt condition) (Figure 3A). Indeed, analysis of H3K27me3 distribution around the Transcription Start Sites (TSS) and along the body of genes indicated a decrease of this repressive mark in *Lmna* Δ8-11 -/- MuSCs compared to wt (Figure 3B and 3C), which was not accompanied by a statistical decrease in H3K27me3 global levels in MuSCs (Figure S5A and S5B) and in whole muscle (Figure S5C and S5D). In contrast, a deep analysis of H3K27me3 ChIP-seq reads coverage in the intergenic genomic regions between the known H3K27me3 enrichment peaks interestingly showed a higher average coverage in the *Lmna* Δ8-11 -/- MuSCs compared to wt counterparts (Figure 3D). These results are compatible with a diffusion of PcG proteins along the chromatin fibers rather than a complete PcG displacement. To identify the PcG targets mostly affected by Lamin A deficiency, genes were grouped according to their transcription level in wt MuSCs. We thus defined 4 equally sized groups of genes based on expression level quartiles (Figure 3E). For each expression category, we reanalysed the H3K27me3 distribution along the body of genes and the TSS and the percentage of upregulated genes in the *Lmna* Δ8-11 -/- MuSCs (Figure 3E, 3F and S5E). In quartile I we found only a small percentage (0.65%) of upregulated genes in *Lmna* Δ8-11 -/-, suggesting that the H3K27me3 decrease/redistribution is not sufficient to activate transcription in highly repressed genes (Figure 3F, S5E and S6A). In contrast, quartiles II, III and IV are more affected by the diminished H3K27me3 levels in *Lmna* Δ8-11 -/- (Figure 3F, S5E and S6B), showing a percentage of upregulated genes between 5 and 9%. Specifically, we noticed that in wt MuSCs, H3K27me3 ChIP-seq signal enrichment around the TSS and within the body of genes is progressively lower in quartiles of

8

higher expression, as expected (Figure 3F, III and IV quartiles and S5E). However, for *Lmna* Δ8-11 -/- mice the decrease of H3K27me3 signal inside the gene body is relatively less marked than in wt mice, in fact the average enrichment is slightly higher. We quantified and confirmed this observation by considering the ratio of H3K27me3 ChIP-seq enrichment signal at the TSS and 2.5Kb downstream of the TSS, for each gene, in wt and *Lmna* Δ8-11 -/- mice (Figure S7A), showing that this ratio is significantly different for higher expression quartiles (Figure S7B).

Lamin A-dependent PcG redistribution determines de-repression of non-muscle related bivalent genes

The altered PcG binding observed in *Lmna* Δ8-11 -/- MuSCs, prompted us to examine more in detail the bivalent genes, a subgroup of PcG targets whose expression is more susceptible to variations of PcG occupancy (27). Bivalent genes are characterized by the concurrent presence of both H3K27me3 and H3K4me3 marks around TSS and have an intermediate gene expression state (28). We first performed H3K27me3 and H3K4me3 ChIP-seq in wt MuSCs (Figure S8A and S8B) and we defined bivalent genes using the parameters described in (17) for the H3K4me3 window at TSS (Figure S8C). Then, we tested the association between bivalent and up-regulated genes in the Lmna Δ 8-11 -/- by means of the Fisher exact test. We observed a significant over-representation of bivalent genes among up-regulated ones in the Lmna Δ 8-11 -/- MuSCs (Figure 4A). To gain more insights into the biological relevance of deregulated genes in the mutant mice, we performed semantic similarity analysis of all GO terms associated with upregulated genes (Figure 4B) together with GSEA (Figure S8D and S8E). These analyses showed a negative correlation with muscle specification (Figure S8D) together with an acquisition of markers related to lipid metabolic processes (Figure 4B and S8E). Notably, Fisher exact test analysis highlighted a significant overlap between genes

with bivalent promoter and the Lmna Δ8-11 -/- MuSCs up-regulated genes involved in adipogenesis (Figure 4C), suggesting that Lamin A is involved in preserving MuSCs identity by ensuring the correct PcG-mediated transcriptional repression of non-muscle genes.

PPARγ is aberrantly expressed in *Lmna* Δ8-11 -/- dystrophic MuSCs

Given this strong association between bivalent reactivation and adipogenesis markers (Figure 4C), we analysed different lipid-related GO categories, finding among the top GO terms, PPARG (Peroxisome proliferator-activated receptor gamma) (Supplementary Table S1). This master transcription factor for adipose cell differentiation (29, 30) was found statistically upregulated in *Lmna* Δ8-11 -/- MuSCs (FDR< 0.05). Moreover, PPARG gene is a Polycomb target and has a bivalent signature in wt MuSCs (Supplementary Table S1 and Figure S9A). These observations prompted us to analyse PPARG transcriptional deregulation. We stained muscles with PAX7 and PPARγ to directly test if MuSCs displayed aberrant expression of PPARγ in the absence of Lamin A. Strikingly, we found about 10% of *Lmna* Δ8-11 -/- MuSCs that simultaneously express both muscular and adipogenesis markers being PAX7+/ PPARγ+ (Figure 5A and 5B). Accordingly, the genomic region of the PPARG gene showed a decrease of H3K27me3 enrichment around the TSS in the *Lmna* Δ8-11 -/- MuSCs, accompanied by a transcriptional up-regulation (Figure S9B). To evaluate if the aberrant expression of adipogenic genes in MuSCs of mutant mice culminate with fatty infiltration we performed an immunofluorescence for Perilipin 1, a protein present on the surface of lipid droplets (31) (Figure 5C and 5D), on cryosections of muscles derived from 19 days-old *Lmna* Δ8-11 mice. We found large areas of adipose accumulation between myofibers of LaminA/C +/- and -/- muscles, which were instead undetectable in the wt mice. Considering the key role of PcG proteins in mediating the formation of chromatin loop structures (32, 33), we

reasoned that the loss of H3K27me3 and transcriptional up-regulation of PPARG locus could be related to the alteration of chromatin 3D structure. The genome 3D architecture is organized in structurally separated Topologically Associated Domains (TADs), chromosomal structures that favour intra-domain looping interactions (34). TADs can be identified by genome-wide chromosome conformation capture (Hi-C) and are largely conserved across different cell types. We verified that the PPARG locus is included in a TAD encompassing a region extending also upstream of the PPARG locus itself, using high-resolution Hi-C data on mouse embryonic stem cells (35) and the 3D Genome Browser (36) (Figure S10). Then, we performed 3D multicolor DNA FISH analysis on pre-fixed MuSCs using one BAC probe overlapping the PPARG promoter and a second probe annealing at the other TAD border. We observed an overlap of the signals from the two regions in the wt *Lmna* Δ8-11 +/+ MuSCs that indicates the presence of a DNA looping *in cis* (Figure 5E and 5F). By contrast, in *Lmna* Δ8-11 -/- MuSCs the distance between the signals was higher, definitely suggesting the lack of DNA/DNA interaction. Indeed, from the analysis of H3K27me3 ChIPseq tracks we noticed in the *Lmna* Δ8-11 -/- MuSCs a reduction of H3K27me3 peaks upstream the PPARG locus (Figure S10). FISH analysis also highlighted that in wt the entire genomic region is close to the nuclear periphery (Figure 5E and 5G) while in *Lmna* Δ8-11 -/- is re-located in the nuclear interior, suggesting that Lamin A absence interferes with chromatin anchoring to the nuclear lamina and PcG dependent DNA conformation.

Lmna Δ8-11 -/- MuSCs undergo premature senescence

Taken together, these results clearly point towards a role of Lamin A in mediating PcG-transcriptional repression in MuSCs to safeguard their identity and regenerative capacity. This lack of cell identity and the impairment of self-renewal displayed by *Lmna* Δ8-11 -/- MuSCs are all features reminiscent of the phenotype described for Ezh2-null MuSCs (24). Moreover, the impairment in self-renewal and the progressive

decline of MuSCs pool are also typical traits of aged MuSCs (37) in which both Lamin A/C and PcG proteins play a key role (38, 39). A major cellular mechanism that ensures self-renewal and hence the maintenance of the MuSC pool is the asymmetric division (40). At the molecular level, in aged mice, the accumulation of activated form of P38 (phospho-p38, Ph-P38) and its symmetric distribution in MuSC doublets heavily compromise the self-renewal capacity leading to MuSCs functional decline (41, 42). To test whether premature exhaustion of quiescent *Lmna* Δ8-11 -/- MuSCs cells could be ascribed to a defective asymmetric division, we stained myofibers-associated MuSCs for Ph-p38 after 48h of culture, a timing at which, 19 days-post-natal myofibers formed MuSCs-derived doublets (Figure 6A). In contrast to wt, *Lmna* Δ8-11 -/- MuSC doublets showed a preferential symmetric distribution of ph-p38, quantified by relative fluorescence intensity (Figure 6A and 6B) often accompanied by a planar orientation with respect to myofibers (see additional methods) (Figure 6C). This highlights problems in asymmetric division, which should be instead characterized by apico-basal orientation (43). In line with this result, in *Lmna* Δ8-11 -/- muscle sections we found higher amount of Ph-P38+ (Figure S11A and S11B) MuSCs and sign of genomic instability, as measured by increased γH2AX DNA repair signal foci (Figure S11C and S11D), not accompanied by apoptosis or necrosis as evidenced by Annexin staining (Figure S12A). To test if defective asymmetric division is associated to premature senescence we then analysed RNAseq to determine if *Lmna* Δ8-11 -/- MuSCs share the same transcriptional signature of MuSCs isolated from aged mice. We performed a GSEA using two different RNA datasets from MuSCs of 24 months old mice (25, 44) and *Lmna* Δ8-11 -/- up-regulated genes. In line with our hypothesis, we found that 19 days-old *Lmna* Δ8-11 -/- MuSCs present an upregulated transcriptome similar to 20-24-months-old MuSCs (Figure 6D and S12B), but different from geriatric 28-32-months-old MuSCs (Figure S12C). At the molecular level, the senescence program is supported by upregulation of some PcG-regulated Cyclin-dependent Kinase Inhibitors (CDKIs) (45)

as p21, involved in cellular senescence and in cell cycle arrest. p21 maintains the viability of DNA damage-induced senescent cells (46) and aberrant expression of p21 has been observed in EDMD derived human myoblasts (47). ChIP-seq and RNA-seq analysis of *Cdkn1a*/p21 locus showed a displacement of Ezh2 from the promoter accompanied by an upregulation of p21 transcript in *Lmna* Δ8-11 -/- MuSCs (Figure 6E).

Genetic ablation of *Cdkn2a* locus partially rescues self-renewal defects in *Lmna* Δ8-11 -/- dystrophic mice.

To further corroborate our findings, we also analysed the *Cdkn2a* locus, a PcG target primarily involved in muscular senescence (44) (Figure S13A). Two transcripts, p16^{INK4a} and p19^{ARF} originate from *Cdkn2a* locus (48). Interestingly, it has been recently reported that p16^{INK4a} expression is a second event, subsequent to p21 upregulation, in the cellular senescence progression (49). In line with these observations, p16^{INK4a} expression is specifically induced in geriatric 28-32-months-old MuSCs (not in 24-months-old MuSCs) (44). Moreover, depletion of p16^{INK4a} is sufficient to reduce senescence-associated gene expression in geriatric MuSCs. RNA-seq and qRT-PCR on 19-days old *Lmna* Δ8-11 -/- MuSCs did not reveal any transcription of p16^{INK4a} in wt or *Lmna* Δ8-11 -/- (Figure 7A). However, qRT-PCR analysis performed in older mice (26 days from birth), revealed higher levels of p16^{INK4a} transcript in *Lmna* Δ8-11 -/- MuSCs and whole muscles compared to the wt counterpart (Figure 7A), suggesting a transition during dystrophy progression toward geriatric condition. We thus decided to test whether the genetic ablation of *Cdkn2a* locus could reverse *Lmna* Δ8-11 -/- MuSCs premature aging, by crossing *Lmna* Δ8-11 +/- with *Cdkn2a* -/- mice (50). Analysis performed in *Lmna* Δ8-11 +/+ background showed no differences in the percentage of QSCs and ASCs, nor on CSA, suggesting that *Cdkn2a* is dispensable for post-natal muscle development (Figure 7B, 7C and 7D; *LMNA+/+*). On the other hand, *Cdkn2a Lmna* Δ8-11 -/- mice partially

rescued the quiescent MuSC pool and CSA defects observed in the absence of Lamin A (Figure 7B, 7C and 7D; *LMNA-/-;* S13B and S13C) emphasizing that Lamin A-dependent muscular dystrophy might be due to progressive MuSCs functional decline caused by acquisition of premature aging features.

Discussion

Lamin A-dependent muscular dystrophy pathogenesis has been classically ascribed to nuclear fragility that renders myonuclei more prone to mechanical stress and damage imposed by myofibre contraction (4). However, the evidence that Lamin A/C is expressed also by MuSCs has led to suggest that satellite cell dysfunction might contribute to EDMD progression (51), yet experimental evidence of this hypothesis was still lacking.

Cell fate choice during muscle differentiation is governed by epigenetic factors controlling the sequential restriction of transcriptional programs (52). Any dysfunction in this finely tuned epigenetic regulation could lead to impaired or aberrant cell fate determination (53). Here, we show that Lamin A/C is indeed crucial to preserve MuSCs identity and regenerative capacity. We demonstrate that cell-autonomous Lamin A-dependent Polycomb dysfunction leads to MuSCs functional decline, which culminate with impaired regenerative capacity and dystrophic phenotype (Figure 1). Traditionally, the role of Lamin A/C in muscle differentiation has been considered to cause defects in muscle differentiation (54, 55). However, in other conditions, MuSCs from Lamin A/C null mice showed a normal ability to differentiate and to form myotubes (20, 56). By moving the viewpoint from differentiation to cell identity we now propose that in the absence of Lamin A/C, a portion of MuSCs derails from their fate affecting the quiescent MuSCs pool. At the molecular level, we described a mechanism of Lamin A-dependent deregulation of PcG targets showing the spreading of repressive marks along the chromatin fiber (Figure 3), with lack of the expected higher order structures and consequent de-repression of bivalent genes

14

(Figure 4, 5 and 8). Recently it has been proposed that PcG domains can have distinct size and boundaries characteristics (57): upon differentiation, loci directly involved in fate specification lose PcG-mediated looping interactions, allowing new active promoter/enhancer interactions. In parallel, other PcG domains, such as the Hox clusters, do not change their 3D architecture. Our findings further corroborate this hypothesis showing that the stability of PcG-interacting domains correlates with PcG occupancy and depends on Lamin A (Figure 5 and 8). PcG dysfunctions drive *Lmna* Δ8-11 -/- MuSCs toward two fates not mutually exclusive (Figure 8): lack of cell identity, highlighted by the presence of MuSCs co-expressing muscle and adipogenic markers (Figure 4 and 5), and premature senescence, as shown by defects in asymmetric division and accumulation of Ph-P38 and γH2AX (Figure 6 and S11). These epigenetic alterations determine a progressive decline in MuSCs self-renewal that accompanies the muscular dystrophy progression (Figure 1), ultimately leading to a geriatric condition characterized by the expression of p16^{INK4a} from *Cdkn2a* locus (Figure 7) (58). Genetic ablation of *Cdkn2a* locus can recover some muscular dystrophy defects of the *Lmna* Δ8-11 -/- mouse (Figure 7) thus supporting the hypothesis that dystrophic and aging muscles share a dysfunction of epigenetic mechanisms controlling cell cycle and fate decision of MuSCs. Our findings corroborate recent evidence on PcG dysfunction in human disease (19), showing that PcG alterations contribute to pathology progression and severity in EDMD. This will further stimulate future studies on the role of PcG proteins in the dynamics of stem cell niche, when embedded in a pathological environment.

Methods

Animals

Heterozygous B6.129S1(Cg)-*Lmnatm1Stw*/BkknJ mice (*Lmna* Δ8-11 +/-) (21) and *Cdkn2a* +/- mice (50) were used.

Satellite cells extraction, apoptosis evaluation and multiple injuries

Hind-limb muscle were isolated from sacrificed mice and digested 120 minutes in 2,4 U/ml of Dispase II (Roche, 04942078001), 2 ug/ml of Collagenase A (Roche, 1013586001), 0,2 mM CaCl2 (Sigma, C5670), 4 mM MgCl2 (Sigma, M8266), 10 ng/ml DNase I (Roche, 1014159001) in PBS1X (Euroclone, ECB4004L) at 37°C in a water bath. The sample were resuspended in HBSS (Gibco, 14025-050) supplemented with 0,1% BSA (Sigma, A7030). Cell suspension was serially filtered with 70 (Falcon, 352350) and 40 μm (Falcon, 352340), stained with antibodies indicated in supplementary table S2: PB-CD45 1:50, PB-CD31 1:50, PB-Ter119 1:50, FITC-Sca1 1:50, APC-α7integrin 1:200 and sorted with BD FACS ARIA III for: PB-CD45$^-$/ PB-CD31$^-$/ PB-Ter119$^-$/ FITC-Sca1$^-$/ APC-α7integrin$^+$.

For multiple injury experiment, 20 μl of Cardiotoxin (CTX) 10 μM (Latoxan, L8102) were injected in TA muscle each week for 3 weeks. TA muscle was harvested one week after the last CTX injection.

For apoptosis assay we stained MuSCs with Annexin. 15-20K of satellite cells were washed in 1 mL cold PBS 1X up, centrifuged 7 minutes at 400g and incubated 20 minutes at room temperature in the dark with 100 μL Annexin V FITC buffer (FITC Annexin V Apoptosis Detection Kit I-ref. 556547). Then, samples were washed with 500 μL of cold PBS 1X, centrifuged 7 minutes at 400g and incubated 15 minutes at room temperature in the dark with 300 μL of cold PBS 1X containing 5 μL of Propidium iodide. Samples were analyzed at BD FACS-CANTO (voltage FSC=357, SSC=462, medium flow to acquire, 300-400 events/second).

Immunofluorescence

On muscle sections: *Tibialis Anterior* (TA) muscles were embedded in Killik (Bio-Optica, 05-9801), immediately frozen in pre-cooled isopentane (Sigma, 277258) and sectioned (Leica CM1850 cryostat) at 8 μm thin. Sections were fixed 20 minutes in paraformaldehyde (PFA) 4% (Sigma, P6148) and washed 3x5 minutes in PBS1X (Euroclone, ECB4004L). To permeabilize tissues pre-cooled methanol (Sigma, 322415) at -20°C was added for 6 minutes. Antigen retrieval was performed 2x5 minutes in hot citric acid 80°C (Sigma, C0759) pH6.0 and washed 2x5 minutes in

PBS1X. Sections were blocked 1 h in BSA 4% (Sigma, A7030) followed by incubation 45 minutes with FAB mouse fragment 1:100 (Jackson Immuno Research, 115-007-003)/ PBS1X. Primary antibodies were diluted 1:100 in blocking solution, except for pparγ diluted 1:75, and incubated O/N at 4°C. The day after, sections were washed 3x10 minutes in PBS1X/0,1% BSA and incubated with secondary antibodies in blocking solution 1:200 1h at RT in the dark. Then, sections were washed 3x10 minutes in 0,1% BSA/PBS1X and incubated 2h at RT with Laminin and Pax7 (1:20). After washing 3x10 minutes in PBS1X/0,1% BSA sections were incubated 45 minutes with Cy5 (1:300) and Biotin (1:500) for Pax7 signal amplification. After washing 3x10 minutes in PBS1X, sections were incubated 45 minutes with secondary antibodies Cy3-streptavidin (1:1250). The sections were finally washed 3x10 minutes in PBS1X, stained 5 minutes with dapi (Sigma, D9542), briefly washed twice in PBS1X and mounted on slide with a drop of Prolong Antifade (Life P36930).

On single myofibers: *Tibialis Anterior* (TA), *Soleus* (S), *Gastrocnemius* (G) and *Exstensor Digitorium Longus* (EDL) were isolated from mice and digested 45-50 minutes in 0,2% collagenase type I (Sigma, C0130)/DMEM (Gibco, 10569010) at 37°C. 2 rounds of myofibers washes were performed in pre-coated dishes with 20% FBS (Gibco, 10500064)/DMEM. Myofibers were let grown in DMEM supplemented with 20% FBS, 1% Chicken Embryo extract (Seralab, CE650-DL) and 1% Penicillin/Streptomycin (Euroclone, ECB 3001) for 48h or 96h changing the medium only after 72h. Myofibers were collected in 2ml tubes pre-coated with 10% FBS/PBS1X and fixed 15 minutes with 4%PFA followed by 3 washes in PBS1X. Permeabilization was performed 5 minutes with 0,5% Triton X-100 (Sigma, 93443)/PBS1X followed by 2 washes in PBS1X. Myofibers were incubated 1h in blocking solution (10% of FBS/PBS1X). Primary antibodies were incubated in blocking solution ON at 4°C. The day after myofibers were washed in 0,25% tween/PBS1X twice and incubated 60 minutes with secondary antibodies in blocking solution. Fibers were washed in 0,1% tween/PBS1X, incubate 5 min with dapi, briefly washed twice in PBS1X and mounted on slide with a drop of Prolong Antifade (Thermofisher, P36970).

On satellite cells: In order to preserve the integrity of chromatin architecture, Muscular stem (Satellite) Cells (MuSCs) suspension was fixed in 1% PFA for 9 minutes and quenched with 125 mM Glycine (Sigma, 8898) before FACS staining and sorting. SC cells were placed on pre- Poly-L-lisined coverslips (Sigma, P8920) at density of 100.000/mL for 30 minutes at RT. Coverslips were fixed with PFA at 4%/PBS for 10 minute at RT. Then, cells were washed in 2X5 minutes in 0,05% Triton X-100/PBS 1X, permeabilized with 0,5% Triton X-100/PBS1X for 10 minutes

and rinsed in PBS 1X. The slides were let in 20% Glycerol (Sigma, G5516)/PBS 1X at least 60 minutes followed by 4 round of freeze and thaw: freezed on dry ice (30 seconds) and thawed in 20% Glycerol/PBS 1X at RT. Slides were washed 2X5 minutes in 0,05% Triton X-100 in PBS 1X, 1x5 minutes 0,5% Triton X-100/PBS1X, incubated in HCl 0,1M (Sigma, H1758) for 15 minutes and rinsed in PBS 1X. Aspecific signals were blocked with 1% BSA/PBS1X for 30 minutes at room temperature. Reaction with primary antibodies Ezh2 diluted 1:100 in blocking solution was performed 12–16 h at 4°C; Lamin A/C diluted 1:200 in blocking solution was performed the day after at room temperature for 2 hour. Secondary antibodies were diluted 1:200 in blocking solution for 1 h at room temperature. Washes were done in PBS1X. DNA was counterstained with dapi, and glasses were mounted in Prolong Antifade. Primary antibodies are listed in supplementary table S2. Secondary antibodies were from Jackson Immuno Research: Alexa 488 (711-545-152); Cy5 1:300 (111-115-144); Cy3-streptavidin (016-160-084); Alexa 594 (711-545-150).

Three-dimensional multicolor DNA FISH

To produce probes for 3D multicolor DNA FISH we used the following BAC DNA clones (BACPAC Resources Program, CHORI): CH29-101F16 (for Pparγ) and CH29-555O5 (for the upstream region of Pparγ). 1-3 µg of BAC DNA were labelled with dig-dUTP (Roche, 11093088910) (for the upstream region of Pparγ) or cy3-dUTP (Thermo Fisher Scientific, C11401) (for Pparγ) through nick translation in 50 µl of Labelling mix buffer (0.02 mM C-G-A dNTPs: Euroclone, EMR273025, EMR274025, EMR272025 respectively, 0.01 mM dTTP Euroclone EMR275025, 0.01 mM labelled dUTP, 50 mM Tris-HCl pH 7.8, 5 mM MgCl2, 10 mM b-mercaptoethanol, 10 ng/µl Bovine serum albumin (BSA), 0.05-0.1 U/µl DNA Polymerase I (Thermo Fisher Scientific, 18010-017), 0.004-0.001 U/µl Amplification Grade DNase I (Sigma, D5307) for 30 min-2 h at 16 °C, to obtain an average probe size of 50 bp. Probes were collected by ethanol precipitation, resuspended in 10 mM Tris-HCl pH 7.5 and then quantified using a Nanodrop 1000 Spectrophotometer (Thermo Fisher Scientific). For a single experiment 100-300 ng of each probe was precipitated with 3.5 µg of Mouse Cot-1 DNA (Thermo Fisher Scientific, 18440-016) and 20 µg of Deoxyribonucleic acid, single stranded from salmon testes (Sigma, D7656), and then resuspended in 6 µl of Hybridization solution (50% formamide pH 7.0 (FA)/2X SSC/10% Dextran sulfate). Pre-fixed Satellite cells Cells were plated directly on poly-L-Lisyned coverslips and fixed with 4% Paraformaldehyde (PFA) in 1X PBS and TWEEN 20 0.1% (PBS-T) for 10 min at room temperature. During the

last minute few drops of 0.5% Triton X-100 in 1X PBS (PBS) were added and then cells were washed with 0.01% Triton X-100 in PBS three times for 3 min at room temperature. Cells were first permeabilized with 0.5% Triton X-100 in PBS for 10 min at room temperature. In order to remove RNA, samples were treated with RNase Cocktail Enzyme Mix (Thermo Fisher Scientific, AM2288) for 1 h at 37 °C. Cells were subjected to other steps of permeabilization with 20% Glycerol in PBS overnight at room temperature, followed by four cycles of freeze and thaw interleaved by soak with 20% Glycerol in PBS. Permeabilized cells were washed with PBS three times for 10 min at room temperature. Cells were then incubated in 0.1 M HCl for 5 min at room temperature, followed by a rinse with 2X SSC and then incubated in 50% FA in 2X SSC for at least 30 min at room temperature. Slides were equilibrated in 2X SSC for 2 min, washed in PBS for 3 min and then treated with 0.0025-0.0075% pepsin in 0.01-0.03 N HCl for 2-4 min at room temperature to eliminate cytoskeleton. Pepsin was inactivated with 50 mM MgCl2 in PBS twice for 5 min. Nuclei were post-fixed with 1% PFA in PBS for 1 min, washed with PBS for 5 min and with 2X SSC twice, and then back to 50% FA in 2X SSC for at least 30 min at room temperature. Hybridization solution was loaded on a clean microscopic slide, coverslip with nuclei was turned upside down on the drop of hybridization mixture and sealed with rubber cement. Samples were denatured for 4 min at 75 °C and leaved to hybridize in a metallic box floating in a 37 °C water bath overnight. Samples were washed with 2X SSC three times for 5 min at 37 °C and with 0.1X SSC three times for 5 min at 60 °C, followed a rinse with 0.2% TWEEN 20 in 4X SSC. Aspecific binding sites were blocked with Blocking solution (4% BSA in 4X SSC, 0.2% TWEEN 20) for 20 min at 37 °C. Samples were then incubated in the appropriate concentration of Streptavidin, DyLight 488 Labeled Anti-Digoxigenin/Digoxin (Vector Laboratories, DI-7488) (1:100) diluted in Blocking solution for 35 min in a dark and wet chamber at 37 °C. Samples were washed with 0.2% TWEEN 20 in 4X SSC three times for 3 min at 37 °C, equilibrated in PBS and post-fixed with 2% formaldehyde in PBS for 10 min at room temperature. Finally, the 3D-fixed nuclei were washed with PBS three times for 5 min at room temperature, counterstained with 1 ng/µl DAPI in PBS for 10 min at room temperature and washed with PBS two times for 5 min at room temperature. Coverslips were mounted. An Eclipse Ti-E (Nikon Instruments) microscope was used to scan the nuclei, with an axial distance of between 0.2-0.25 micron consecutive sections.

Histone extraction and Western blot

Total proteins were prepared starting from quadriceps muscle. Muscles were homogenized on ice with tissue ruptor (Qiagen, 902756) in 1ml of extraction buffer (50 mM Tris HCl, pH 7.5, 150mM NaCl, 1 mM EDTA pH 8.0, 0,1% SDS, 1% Np40 (Sigma, 74385), 0,5% Sodium deoxycholate (Sigma, D6750) 1× protease Inhibitors (Roche, 04693132001) 2 mM PMSF (Sigma, 93482), 1 mM NaF (Sigma, s7920); 1 mM Na3VO4). After 30 minutes in ice 3 pulses of 10 seconds sonication at 30% amplitude were performed with Branson digital sonifier 250 to allow dissociation of protein from chromatin and solubilization. Extracts were analyzed by SDS-PAGE using a 8–10% gel (29:1 acrylamide solution Sigma, 01708). For histone extractions approximately 2.000.000 of freshly isolated MuSCs was collected and resuspended in 15uL of 0.2 N HCl with 1× protease Inhibitors (Roche, 04693132001) 2 mM PMSF (Sigma, 93482), 1 mM NaF (Sigma, s7920); 1 mM Na3VO4) and incubated overnight at 4°C with constant rocking. The supernatant was run on 4-12% bis-tris Acrylamide gel (Thermo Fisher Scientific, NW04125).
Primary antibodies are listed in supplementary table S2.

RNA-seq

Total RNA from freshly isolated satellite cells from 3 mice for each genotype was extracted in TRI-Reagent (Sigma, T9424) following the relative guidelines. Libraries were prepared using the Illumina TruSeq Stranded Total RNA with Ribo-Zero GOLD kit and were quality controlled with an Agilent Bioanalyzer at the Sequencing Facility of the Institute of Applied Genomics (IGA, Udine, Italy). 125 bp reads were produced using an Illumina HiSeq2500 machine in paired-end mode to reach a sequencing depth of about 30 million reads for each sample. RTPCR were performed on total RNA extracted from single mouse. Primers sequences: gapdh: gtatgtcgtggagtctactgg, tcgtggttcacacccatcac; p16: gtgtgcatgacgtgcggg, cagttcgaatctgcaccgtag; p19: gctctggctttcgtgaacatg, tcgaatctgcaccgtagttgag; p21: acggaggcagaccagcct, acacagagtgagggctaagg.

ChIP-seq

For ChIP analysis, satellite cells from pools of 6-9 mice were used and prefixed as previously described (Immunofluorescence section). Isolated satellite cells were resuspended in SDS buffer (100 mM NaCl, 50mM TrisHCl pH8.1, 5 mM EDTA, 0.2% NaN$_3$, 0.5% SDS) and stored at -80°C (100 µL/10^6 cells). 2-2.5*10^6 of fixed cells/experiment were thawed on ice, resuspended in fresh SDS buffer and incubated at 4°C in mild agitation for 3 hours, passing them through a 0.50x16mm syringe needle every hour. Solution was then adjusted to IP Buffer composition (100

mM Tris pH 8.6, 0.3% SDS, 1.7% Triton X-100, 5 mM EDTA) and cells were sonicated with Branson Digital Sonifier to 200 bp fragments. For spike-in experiments, a 5% of sheared drosophila chromatin was added to each sample. The 2% of the total volume from each sample was taken as input chromatin. The remaining fragmented chromatin was incubated with 1 mM PMSF (Sigma, 93482) and 4 µg of the antibody of interest on a rotating wheel at 4°C overnight. Primary antibodies used were: H3K27me3 (Millipore 07-449) and H3K4me3 (Millipore 07-473). The next day, protein G beads (Life Technology, 1004D) were added (80 µL) and samples were incubated for additional 2 hours on the rotating wheel at 4°C. The beads were washed with Low Salt solution (150 mM NaCl, 20 mM TrisHCl pH 8.0, 2 mM EDTA, 0.1% SDS, 1% Triton X-100), High Salt solution (500 mM NaCl, 20 mM TrisHCl pH 8.0, 2 mM EDTA, 0.1% SDS, 1% Triton X-100), Low Salt solution and then TE NaCl (50 mM NaCl, 10 mM TrisHCl pH8.0, 1 mM EDTA). Crosslinking was reversed by incubating the beads at 65°C overnight in Elution buffer (50 mM TrisHCl pH 8.0, 10 mM EDTA, 1% SDS). Input chromatin was also decrosslinked in Elution buffer overnight at 65°C. The next day, all samples were diluted with one volume of TE 10:1, treated with 0.2 ug/mL RNase A (Sigma R6513) for 2 hours at 37°C and then with 0.2ug/mL Proteinase K (Sigma P2308) for 2 hours at 55°C. DNA was isolated through standard phenol/chloroform extraction, followed by precipitation and resuspension in 31 µL of 10 mM Tris-HCl pH 8.0. Before library construction, ChIP were validated using the primers: hoxd9 ggataatcgcctaggtgtgactt, catctcttcttgcctctctggg and pax7prom gcgacccctgaggaaaa, cgaaaagaagtctccaacgagtatt. Libraries for IP and reference input DNA were created for each sample using the automation instrument Biomek FX (Beckman Coulter), then qualitatively and quantitatively checked using Agilent High Sensitivity DNA Kit (Agilent Technologies, 5067-4627) on a Bioanalyzer 2100 (Agilent Technologies). Libraries with distinct adapter indexes were multiplexed and, after cluster generation on FlowCell, were sequenced for 50 bases in the single read mode on a HiSeq 2000 sequencer at the IEO Genomic Unit in Milan.

Real-time PCR analysis

Total RNA was extracted from satellite cells using Maxwell RSC miRNA tissue kit (Promega, AS1460), while total RNA from muscle tissues was extracted using TriReagent (Sigma-Aldrich, T9424). 1ug of RNA from each sample was subjected to cDNA synthesis using QuantiTect reverse transcription kit (Qiagen, 205313) and amplified in the presence of 8 ul of SYBR select master mix (Thermo fisher, 4472908). Expression was calculated by normalizing on GAPDH and relative to

the average of the wild type controls samples. Primer sequences used for transcriptional analyses, mouse: mRTP21 5'-acggaggcagaccagcct-3', 5'-acacagagtgagggctaagg-3'; mrtezh2 5'-caaatacatgtgcagctttctg-3', 5'-atgcctatcctgtggtcacc-3'; mrtpparg 5'-ttgctgaacgtgaagcccatcgag-3', 5'-gtccttgtagatctcctggagcag-3'; mrtp16 5'-gtgtgcatgacgtgcggg-3', 5'-cagttcgaatctgcaccgtag-3'; mrtp19 5'-gctctggctttcgtgaacatg-3', 5'-tcgaatctgcaccgtagttgag-3'; mrtgapdh 5'-gtatgtcgtggagtctactgg-3', 5'-tcgtggttcacacccatcac-3'.

Bioinformatics and image analysis
See additional methods.

Data availability
The datasets generated during the current study are available in the GEO repository with accession number GSE123725.

Statistics
All the data are represented using Graph Pad prism 6. The sample size (n) is described for each experiment in the relative figure legend. Multiple comparison between three o more groups were made using one way Anova or two way Anova with significance as P value <0,05 (*), P value < 0,01 (**), P value <0,001 (***).

Study approval
Heterozygous B6.129S1(Cg)-*Lmnatm1Stw*/BkknJ mice (*Lmna* Δ8-11 +/-) (21) and *Cdkn2a* +/- mice (50) were used. All the experimental procedures were performed under the ethical approval of the Italian Ministry of Health and the Institutional Animal Care and Use Committee (authorization n. 83/2019-PR). The animals were maintained in an authorized facility at San Raffaele Hospital, Milan (authorization n. 127/2012-A) and Santa Lucia Foundation, Rome (authorization n. 9/2006-A).

Author Contributions

C.L. conceived the project and designed experiments. A.B. and C.M. performed

experiments and analysed data. F. L. and D.P. performed and interpreted ChIP-

seq experiments. S.V. performed bioinformatic analysis. G.P., V.R., R.R. and C.B.

performed experiments in mice. A.B., A.C. and B.B. performed and interpreted

FISH experiments. L.A., F.G. and G.O. quantified immunofluorescence and FISH images. M.D.B. performed FACS. F.F. and C.P. analysed ChIPseq data. C.L. supervised the project and analysed data. C.L., A.B. and C.M. wrote the manuscript. All authors edited and approved the manuscript.

References

1.   Shimi T, Kittisopikul M, Tran J, Goldman AE, Adam SA, Zheng Y, Jaqaman K, and Goldman RD. Structural organization of nuclear lamins A, C, B1, and B2 revealed by superresolution microscopy. *Mol Biol Cell.* 2015;26(22):4075-86.
2.   Turgay Y, Eibauer M, Goldman AE, Shimi T, Khayat M, Ben-Harush K, Dubrovsky-Gaupp A, Sapra KT, Goldman RD, and Medalia O. The molecular architecture of lamins in somatic cells. *Nature.* 2017;543(7644):261-4.
3.   van Steensel B, and Belmont AS. Lamina-Associated Domains: Links with Chromosome Architecture, Heterochromatin, and Gene Repression. *Cell.* 2017;169(5):780-91.
4.   Zaremba-Czogalla M, Dubinska-Magiera M, and Rzepecki R. Laminopathies: the molecular background of the disease and the prospects for its treatment. *Cell Mol Biol Lett.* 2011;16(1):114-48.
5.   Kolb T, Maass K, Hergt M, Aebi U, and Herrmann H. Lamin A and lamin C form homodimers and coexist in higher complex forms both in the nucleoplasmic fraction and in the lamina of cultured human cells. *Nucleus.* 2011;2(5):425-33.
6.   Serebryannyy L, and Misteli T. Protein sequestration at the nuclear periphery as a potential regulatory mechanism in premature aging. *J Cell Biol.* 2018;217(1):21-37.
7.   Dubinska-Magiera M, Zaremba-Czogalla M, and Rzepecki R. Muscle development, regeneration and laminopathies: how lamins or lamina-associated proteins can contribute to muscle development, regeneration and disease. *Cell Mol Life Sci.* 2013;70(15):2713-41.
8.   Schuettengruber B, Bourbon HM, Di Croce L, and Cavalli G. Genome Regulation by Polycomb and Trithorax: 70 Years and Counting. *Cell.* 2017;171(1):34-57.
9.   Briand N, and Collas P. Laminopathy-causing lamin A mutations reconfigure lamina-associated domains and local spatial chromatin conformation. *Nucleus.* 2018;9(1):216-26.
10.   Cesarini E, Mozzetta C, Marullo F, Gregoretti F, Gargiulo A, Columbaro M, Cortesi A, Antonelli L, Di Pelino S, Squarzoni S, et al. Lamin A/C sustains PcG protein architecture, maintaining transcriptional repression at target genes. *J Cell Biol.* 2015;211(3):533-51.
11.   Marullo F, Cesarini E, Antonelli L, Gregoretti F, Oliva G, and Lanzuolo C. Nucleoplasmic Lamin A/C and Polycomb group of proteins: an evolutionarily conserved interplay. *Nucleus.* 2016:0.
12.   Oldenburg A, Briand N, Sorensen AL, Cahyani I, Shah A, Moskaug JO, and Collas P. A lipodystrophy-causing lamin A mutant alters conformation and epigenetic regulation of the anti-adipogenic MIR335 locus. *J Cell Biol.* 2017;216(9):2731-43.
13.   Salvarani N, Crasto S, Miragoli M, Bertero A, Paulis M, Kunderfranco P, Serio S, Forni A, Lucarelli C, Dal Ferro M, et al. The K219T-Lamin mutation induces conduction defects through epigenetic inhibition of SCN5A in human cardiac laminopathy. *Nat Commun.* 2019;10(1):2267.

14. Zheng X, Hu J, Yue S, Kristiani L, Kim M, Sauria M, Taylor J, Kim Y, and Zheng Y. Lamins Organize the Global Three-Dimensional Genome from the Nuclear Periphery. *Mol Cell.* 2018;71(5):802-15 e7.

15. Chiacchiera F, Rossi A, Jammula S, Piunti A, Scelfo A, Ordonez-Moran P, Huelsken J, Koseki H, and Pasini D. Polycomb Complex PRC1 Preserves Intestinal Stem Cell Identity by Sustaining Wnt/beta-Catenin Transcriptional Activity. *Cell Stem Cell.* 2016;18(1):91-103.

16. Lapthanasupkul P, Feng J, Mantesso A, Takada-Horisawa Y, Vidal M, Koseki H, Wang L, An Z, Miletich I, and Sharpe PT. Ring1a/b polycomb proteins regulate the mesenchymal stem cell niche in continuously growing incisors. *Dev Biol.* 2012;367(2):140-53.

17. Bernstein BE, Mikkelsen TS, Xie X, Kamal M, Huebert DJ, Cuff J, Fry B, Meissner A, Wernig M, Plath K, et al. A bivalent chromatin structure marks key developmental genes in embryonic stem cells. *Cell.* 2006;125(2):315-26.

18. Morata G, and Herrera SC. Cell reprogramming during regeneration in Drosophila: transgression of compartment boundaries. *Curr Opin Genet Dev.* 2016;40(11-6.

19. Lu TT, Heyne S, Dror E, Casas E, Leonhardt L, Boenke T, Yang CH, Sagar, Arrigoni L, Dalgaard K, et al. The Polycomb-Dependent Epigenome Controls beta Cell Dysfunction, Dedifferentiation, and Diabetes. *Cell Metab.* 2018;27(6):1294-308 e7.

20. Cohen TV, Gnocchi VF, Cohen JE, Phadke A, Liu H, Ellis JA, Foisner R, Stewart CL, Zammit PS, and Partridge TA. Defective skeletal muscle growth in lamin A/C-deficient mice is rescued by loss of Lap2alpha. *Hum Mol Genet.* 2013;22(14):2852-69.

21. Sullivan T, Escalante-Alcalde D, Bhatt H, Anver M, Bhat N, Nagashima K, Stewart CL, and Burke B. Loss of A-type lamin expression compromises nuclear envelope integrity leading to muscular dystrophy. *J Cell Biol.* 1999;147(5):913-20.

22. Gregoretti F, Cesarini E, Lanzuolo C, Oliva G, and Antonelli L. An Automatic Segmentation Method Combining an Active Contour Model and a Classification Technique for Detecting Polycomb-group Proteinsin High-Throughput Microscopy Images. *Methods Mol Biol.* 2016;1480(181-97.

23. Boonsanay V, Zhang T, Georgieva A, Kostin S, Qi H, Yuan X, Zhou Y, and Braun T. Regulation of Skeletal Muscle Stem Cell Quiescence by Suv4-20h1-Dependent Facultative Heterochromatin Formation. *Cell Stem Cell.* 2016;18(2):229-42.

24. Juan AH, Derfoul A, Feng X, Ryall JG, Dell'Orso S, Pasut A, Zare H, Simone JM, Rudnicki MA, and Sartorelli V. Polycomb EZH2 controls self-renewal and safeguards the transcriptional identity of skeletal muscle stem cells. *Genes Dev.* 2011;25(8):789-94.

25. Liu L, Cheung TH, Charville GW, Hurgo BM, Leavitt T, Shih J, Brunet A, and Rando TA. Chromatin modifications as determinants of muscle stem cell quiescence and chronological aging. *Cell Rep.* 2013;4(1):189-204.

26. Orlando DA, Chen MW, Brown VE, Solanki S, Choi YJ, Olson ER, Fritz CC, Bradner JE, and Guenther MG. Quantitative ChIP-Seq normalization reveals global modulation of the epigenome. *Cell Rep.* 2014;9(3):1163-70.

27. Minoux M, Holwerda S, Vitobello A, Kitazawa T, Kohler H, Stadler MB, and Rijli FM. Gene bivalency at Polycomb domains regulates cranial neural crest positional identity. *Science.* 2017;355(6332).

28. Bernstein E, Duncan EM, Masui O, Gil J, Heard E, and Allis CD. Mouse polycomb proteins bind differentially to methylated histone H3 and RNA and are enriched in facultative heterochromatin. *Mol Cell Biol.* 2006;26(7):2560-9.

29. Barak Y, Nelson MC, Ong ES, Jones YZ, Ruiz-Lozano P, Chien KR, Koder A, and Evans RM. PPAR gamma is required for placental, cardiac, and adipose tissue development. *Mol Cell.* 1999;4(4):585-95.

30. Rosen ED, Sarraf P, Troy AE, Bradwin G, Moore K, Milstone DS, Spiegelman BM, and Mortensen RM. PPAR gamma is required for the differentiation of adipose tissue in vivo and in vitro. *Mol Cell.* 1999;4(4):611-7.

31. Tong J, Li W, Vidal C, Yeo LS, Fatkin D, and Duque G. Lamin A/C deficiency is associated with fat infiltration of muscle and bone. *Mech Ageing Dev.* 2011;132(11-12):552-9.

32. Bantignies F, Roure V, Comet I, Leblanc B, Schuettengruber B, Bonnet J, Tixier V, Mas A, and Cavalli G. Polycomb-Dependent Regulatory Contacts between Distant Hox Loci in Drosophila. *Cell.* 2011;144(2):214-26.

33. Lanzuolo C, Roure V, Dekker J, Bantignies F, and Orlando V. Polycomb response elements mediate the formation of chromosome higher-order structures in the bithorax complex. *Nat Cell Biol.* 2007;9(10):1167-74.

34. Dixon JR, Selvaraj S, Yue F, Kim A, Li Y, Shen Y, Hu M, Liu JS, and Ren B. Topological domains in mammalian genomes identified by analysis of chromatin interactions. *Nature.* 2012;485(7398):376-80.

35. Bonev B, Mendelson Cohen N, Szabo Q, Fritsch L, Papadopoulos GL, Lubling Y, Xu X, Lv X, Hugnot JP, Tanay A, et al. Multiscale 3D Genome Rewiring during Mouse Neural Development. *Cell.* 2017;171(3):557-72 e24.

36. Wang Y, Song F, Zhang B, Zhang L, Xu J, Kuang D, Li D, Choudhary MNK, Li Y, Hu M, et al. The 3D Genome Browser: a web-based browser for visualizing 3D genome organization and long-range chromatin interactions. *Genome Biol.* 2018;19(1):151.

37. Chakkalakal JV, Jones KM, Basson MA, and Brack AS. The aged niche disrupts muscle stem cell quiescence. *Nature.* 2012;490(7420):355-60.

38. Gonzalo S, Kreienkamp R, and Askjaer P. Hutchinson-Gilford Progeria Syndrome: A premature aging disease caused by LMNA gene mutations. *Ageing Res Rev.* 2017;33(18-29.

39. Jacobs JJ, Kieboom K, Marino S, DePinho RA, and van Lohuizen M. The oncogene and Polycomb-group gene bmi-1 regulates cell proliferation and senescence through the ink4a locus. *Nature.* 1999;397(6715):164-8.

40. Chang NC, Chevalier FP, and Rudnicki MA. Satellite Cells in Muscular Dystrophy - Lost in Polarity. *Trends Mol Med.* 2016;22(6):479-96.

41. Bernet JD, Doles JD, Hall JK, Kelly Tanaka K, Carter TA, and Olwin BB. p38 MAPK signaling underlies a cell-autonomous loss of stem cell self-renewal in skeletal muscle of aged mice. *Nat Med.* 2014;20(3):265-71.

42. Cosgrove BD, Gilbert PM, Porpiglia E, Mourkioti F, Lee SP, Corbel SY, Llewellyn ME, Delp SL, and Blau HM. Rejuvenation of the muscle stem cell

population restores strength to injured aged muscles. *Nat Med.* 2014;20(3):255-64.

43. Kuang S, Kuroda K, Le Grand F, and Rudnicki MA. Asymmetric self-renewal and commitment of satellite stem cells in muscle. *Cell.* 2007;129(5):999-1010.

44. Sousa-Victor P, Gutarra S, Garcia-Prat L, Rodriguez-Ubreva J, Ortet L, Ruiz-Bonilla V, Jardi M, Ballestar E, Gonzalez S, Serrano AL, et al. Geriatric muscle stem cells switch reversible quiescence into senescence. *Nature.* 2014;506(7488):316-21.

45. Beguelin W, Rivas MA, Calvo Fernandez MT, Teater M, Purwada A, Redmond D, Shen H, Challman MF, Elemento O, Singh A, et al. EZH2 enables germinal centre formation through epigenetic silencing of CDKN1A and an Rb-E2F1 feedback loop. *Nat Commun.* 2017;8(1):877.

46. Yosef R, Pilpel N, Papismadov N, Gal H, Ovadya Y, Vadai E, Miller S, Porat Z, Ben-Dor S, and Krizhanovsky V. p21 maintains senescent cell viability under persistent DNA damage response by restraining JNK and caspase signaling. *EMBO J.* 2017;36(15):2280-95.

47. Kandert S, Wehnert M, Muller CR, Buendia B, and Dabauvalle MC. Impaired nuclear functions lead to increased senescence and inefficient differentiation in human myoblasts with a dominant p.R545C mutation in the LMNA gene. *Eur J Cell Biol.* 2009;88(10):593-608.

48. Quelle DE, Ashmun RA, Hannon GJ, Rehberger PA, Trono D, Richter KH, Walker C, Beach D, Sherr CJ, and Serrano M. Cloning and characterization of murine p16INK4a and p15INK4b genes. *Oncogene.* 1995;11(4):635-45.

49. Ito T, Teo YV, Evans SA, Neretti N, and Sedivy JM. Regulation of Cellular Senescence by Polycomb Chromatin Modifiers through Distinct DNA Damage- and Histone Methylation-Dependent Pathways. *Cell Rep.* 2018;22(13):3480-92.

50. Serrano M, Lee H, Chin L, Cordon-Cardo C, Beach D, and DePinho RA. Role of the INK4a locus in tumor suppression and cell mortality. *Cell.* 1996;85(1):27-37.

51. Gnocchi VF, Ellis JA, and Zammit PS. Does satellite cell dysfunction contribute to disease progression in Emery-Dreifuss muscular dystrophy? *Biochem Soc Trans.* 2008;36(Pt 6):1344-9.

52. Robinson DCL, and Dilworth FJ. Epigenetic Regulation of Adult Myogenesis. *Curr Top Dev Biol.* 2018;126(235-84.

53. Tosic M, Allen A, Willmann D, Lepper C, Kim J, Duteil D, and Schule R. Lsd1 regulates skeletal muscle regeneration and directs the fate of satellite cells. *Nat Commun.* 2018;9(1):366.

54. Frock RL, Kudlow BA, Evans AM, Jameson SA, Hauschka SD, and Kennedy BK. Lamin A/C and emerin are critical for skeletal muscle satellite cell differentiation. *Genes Dev.* 2006;20(4):486-500.

55. Solovei I, Wang AS, Thanisch K, Schmidt CS, Krebs S, Zwerger M, Cohen TV, Devys D, Foisner R, Peichl L, et al. LBR and lamin A/C sequentially tether peripheral heterochromatin and inversely regulate differentiation. *Cell.* 2013;152(3):584-98.

56. Melcon G, Kozlov S, Cutler DA, Sullivan T, Hernandez L, Zhao P, Mitchell S, Nader G, Bakay M, Rottman JN, et al. Loss of emerin at the nuclear

envelope disrupts the Rb1/E2F and MyoD pathways during muscle regeneration. *Hum Mol Genet.* 2006;15(4):637-51.

57.   Kundu S, Ji F, Sunwoo H, Jain G, Lee JT, Sadreyev RI, Dekker J, and Kingston RE. Polycomb Repressive Complex 1 Generates Discrete Compacted Domains that Change during Differentiation. *Mol Cell.* 2017;65(3):432-46 e5.

58.   Sousa-Victor P, Perdiguero E, and Munoz-Canoves P. Geroconversion of aged muscle stem cells under regenerative pressure. *Cell Cycle.* 2014;13(20):3183-90.
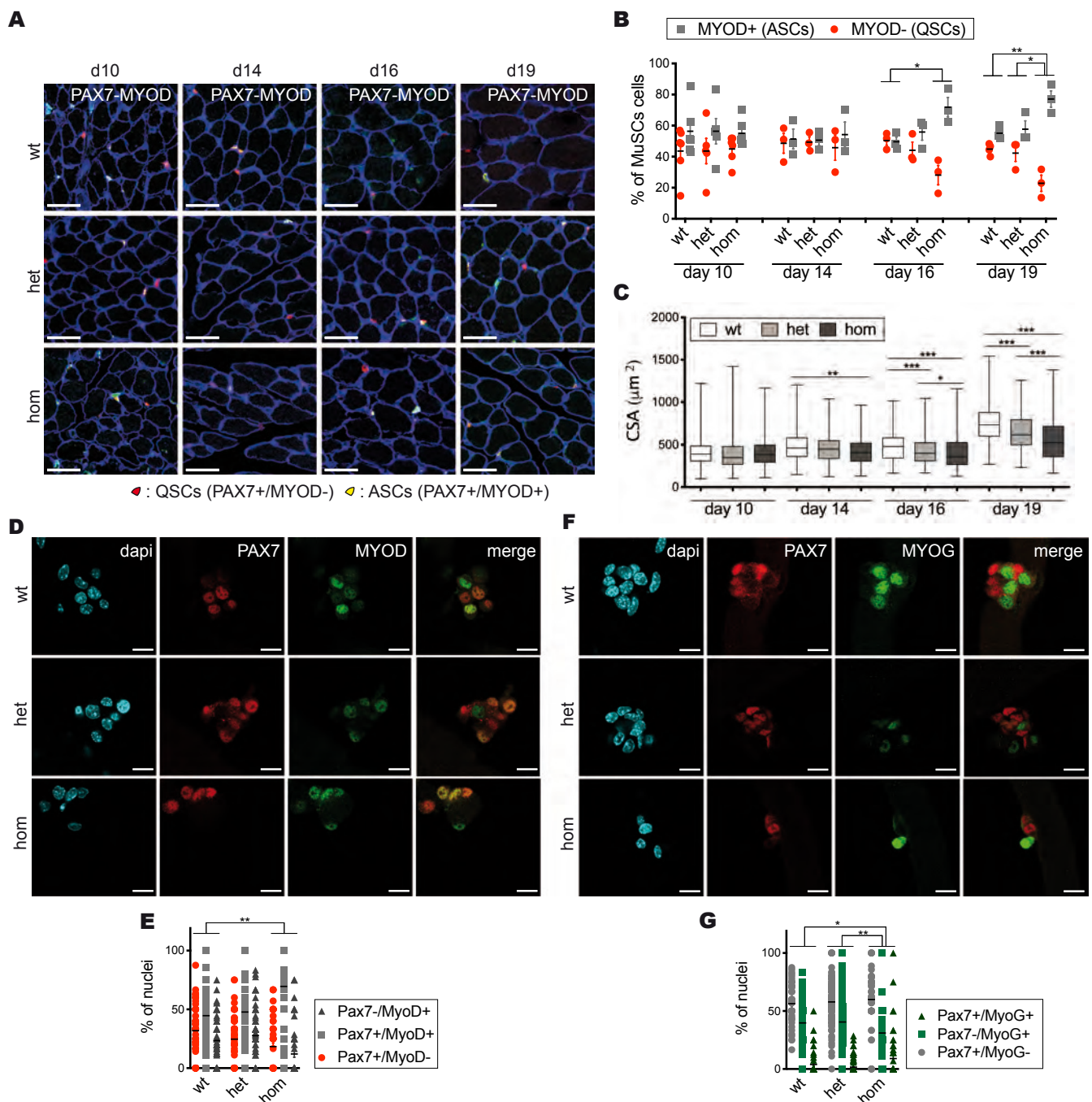
Figure 1. Lamin A regulates MuSC self-renewal.

(A) Immunohistochemical staining in Lmna Δ8-11 mice of PAX7 and MYOD markers at the indicated days of post-natal growth (d10-d19). Basement membrane of muscle fibers was stained with Laminin. Activated, ASCs (PAX7+/MYOD+) and self-renewing, QSCs (PAX7+/MYOD-) MuSCs are shown. Scale bars, 50 μm. (B) Quantification of MuSCs pool composition in (A); n =3-6 animals per genotype (C) Quantification of myofibre size during post-natal growth, evaluated by the Cross Sectional area (CSA). n> 350 fibers, n =3-4 animals per genotype. (D) Immunohistochemical staining of single myofibers extracted from Lmna Δ8-11 mice at d19 and cultured 96h. Activated (PAX7+/MYOD+), self-renewing (PAX7+/MYOD-) and differentiating (PAX7-/MYOD+) cells are shown. Scale bars, 20 μm. (E) Quantification of MuSCs pool composition in (D); n> 50 muscle fibers/ genotype, n= 5-8 animals per genotype. (F) Immunohistochemical staining of single myofibers as in (D). PAX7+/MYOG+, PAX7+/MYOG- and PAX7-/MYOG+ cells are shown. Scale bars, 20 μm. (G) Quantification of MuSCs pool composition in (F); n> 50 muscle fibers/group, n= 3-5 animals per genotype. B, E, G, Data are mean ± s.e.m. C, Data are box with median and whiskers min to max. Statistics by one-way (C) or two-way (B, E, G) analysis of variance (ANOVA) with multiple comparisons. * P < 0.05, * * P < 0.01, * * * P < 0.001; wt= Lmna Δ8-11 +/+; het= Lmna Δ8-11 +/-; hom= Lmna Δ8-11 -/-.
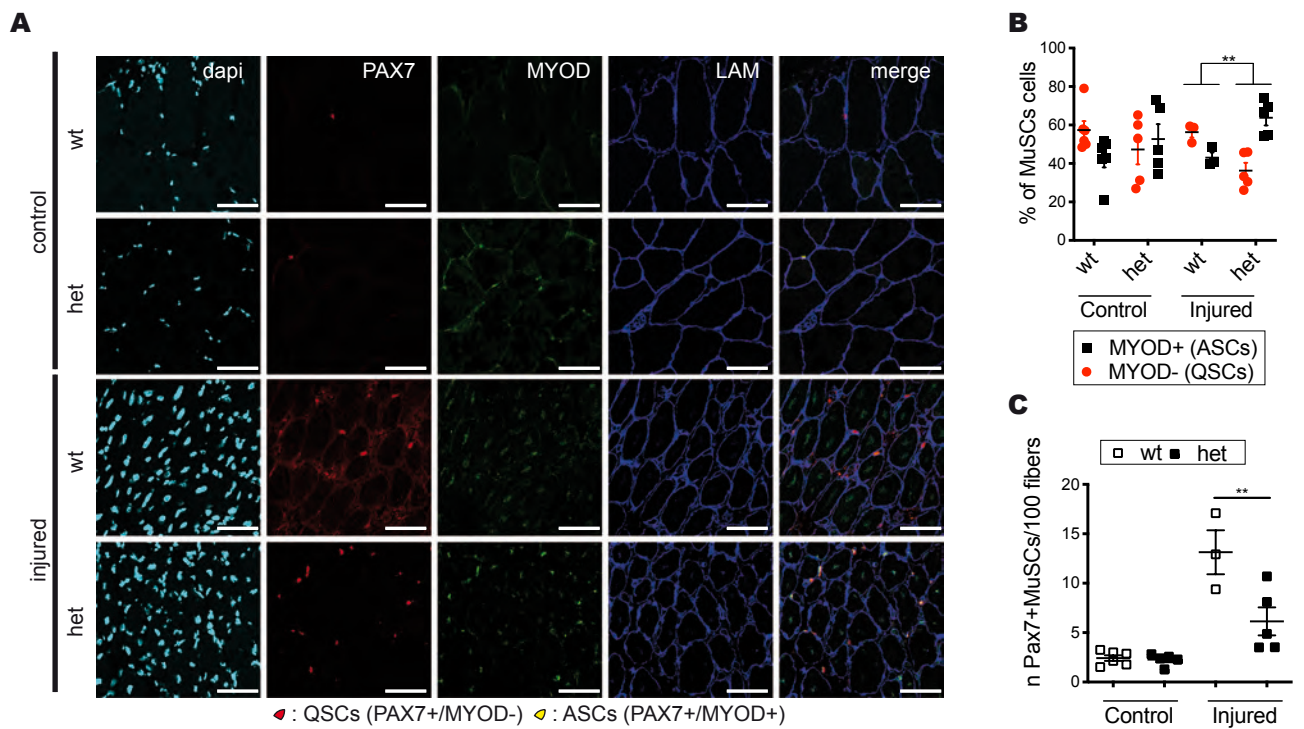
Figure 2. Lamin A levels influence muscle regeneration.

(A) Immunohistochemical staining in adult, injured Lmna Δ8-11 mice of PAX7 and MYOD markers. Basement membrane of muscle fibers was stained with Laminin. Activated, ASCs (PAX7+/MYOD+) and self-renewing, QSCs (PAX7+/MYOD-) MuSCs are shown. Scale bars, 100 μm. (B), Quantification of MuSCs pool composition in (A); n= 3-6 animals per group. (C), Number of Pax7+ MuSCs on 100 fibers for the experiment shown in (A). B, C, Data are mean ± s.e.m. Statistics by one-way (C) or two-way (B) analysis of variance (ANOVA) with multiple comparisons. Statistical comparisons between controls and injured (B, C) were not shown.
* * $P < 0.01$; wt= Lmna Δ8-11 +/+; het= Lmna Δ8-11 +/-.
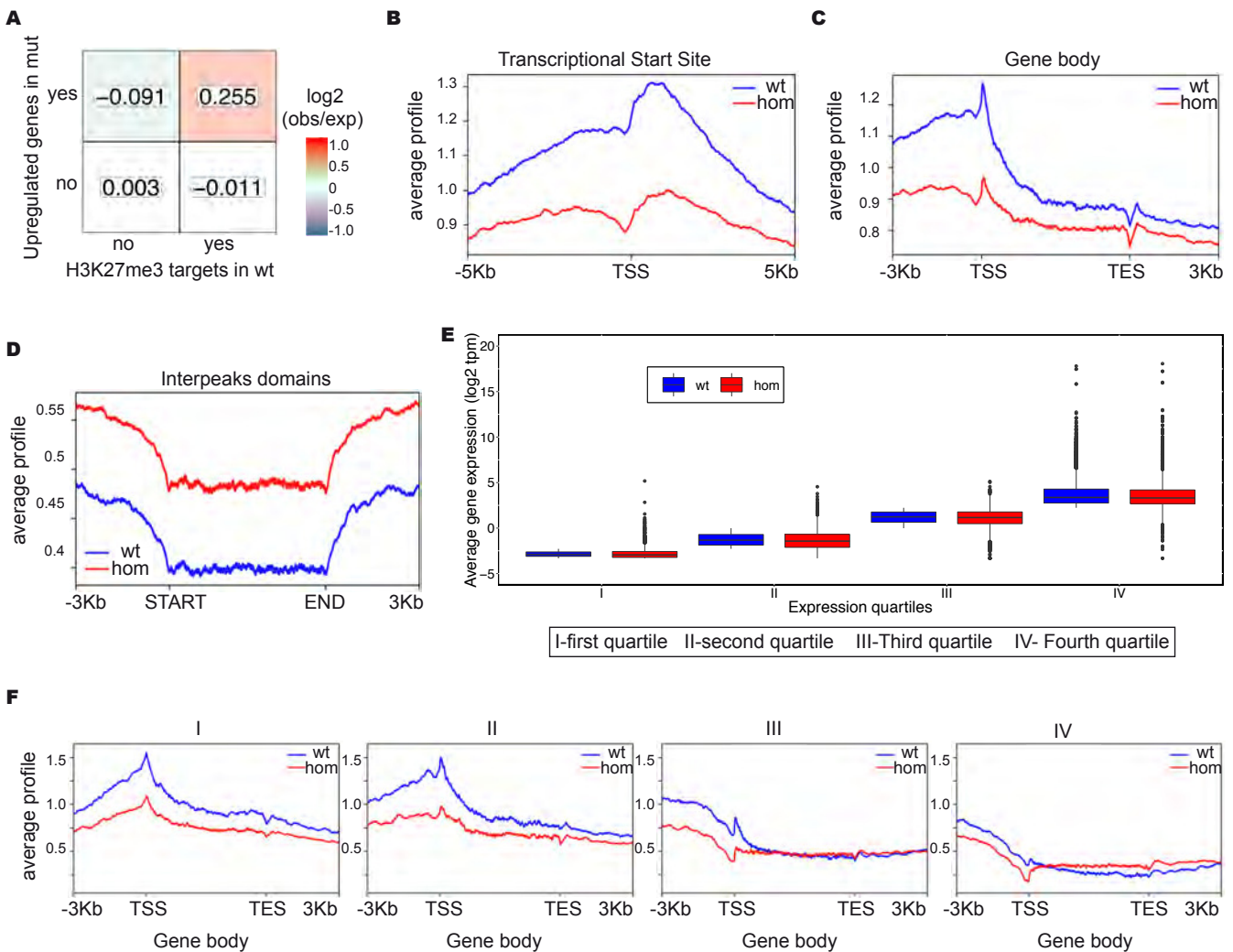
Figure 3. Lmna Δ8-11 -/- dystrophic MuSCs display PcG displacement.

(A) Heatmap reporting log2 ratios of observed over expected (coloured bar) number of genes in the intersections between H3K27me3 targets identified in Lmna Δ8-11 +/+ mice and the up-regulated genes in Lmna Δ8-11 -/- mice. Fisher Exact Test p-value = 2.38e-05. (B, C, D) Average profile of H3K27me3 ChIP-seq signal calculated as the IP/input ratio over annotated mouse genes (B) Average profile of H3K27me3 signal around the TSS. (C) Average profile of H3K27me3 signal along the gene body. TES= annotated transcript end. (D) Average profile of H3K27me3 signal in regions outside H3K27me3 peaks and outside annotated genes. (E) Normalized expression distribution of genes stratified using wt expression level in the 3 biological replicates (see additional methods). Distribution of average log2 transcripts per million (TPM + 0.1) values is plotted for wt and hom. Data in the box extends from the 25th to the 75th percentiles with the median indicated. The upper whisker extends from the hinge to the highest value that is within 1.5 * IQR of the hinge, where IQR is the inter-quartile range, or distance between the first and third quartiles. The lower whisker extends from the hinge to the lowest value within 1.5 * IQR of the hinge. Data beyond the end of the whiskers are outliers and plotted as points. (F) Average profile of H3K27me3 signal (IP/input) along the gene body using gene categories as in panel (E). wt= Lmna Δ8-11 +/+; hom= Lmna Δ8-11 -/-.
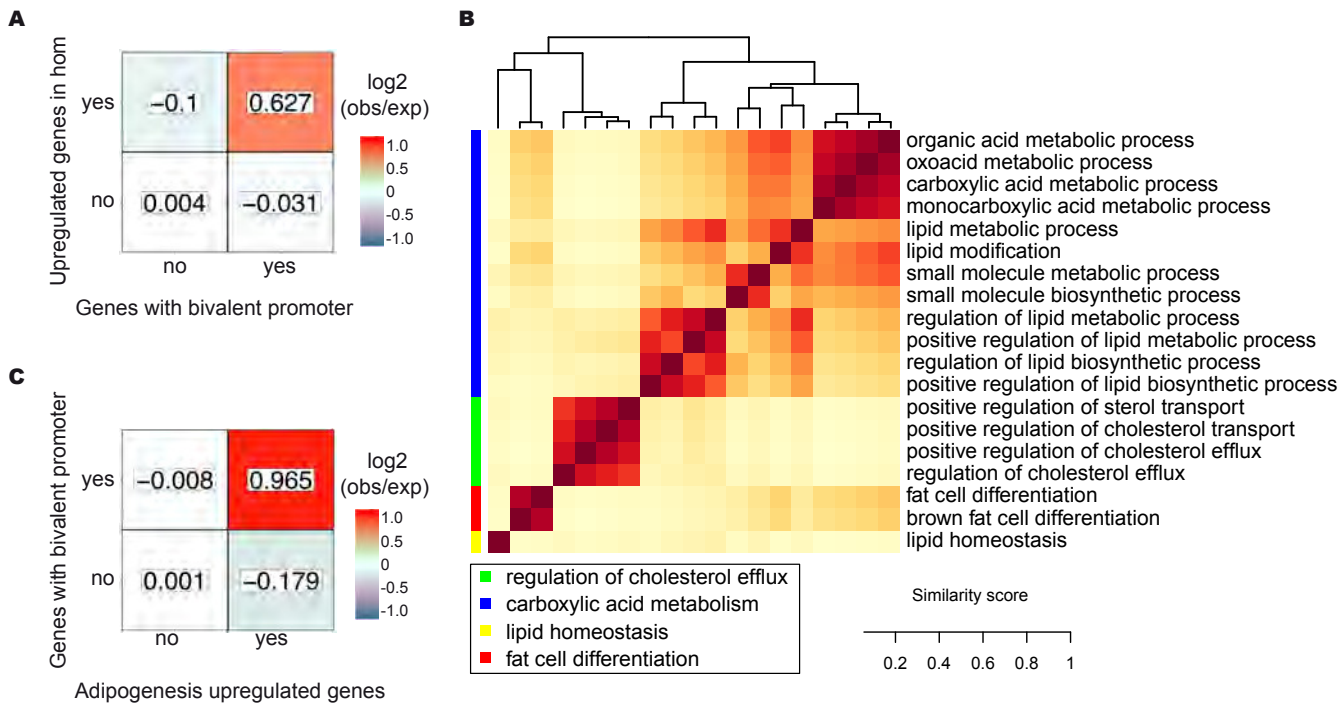
Figure 4. Lamin A-PcG-mediated transcriptional repression preserves MuSCs identity.

(A) Heatmap reporting log2 ratios of observed over expected number of genes (coloured bar) in the intersections between bivalent promoters identified in wt satellite cells and the up-regulated genes in Lmna Δ8-11 -/- mice. Fisher's Exact Test p-value = 4.57e-07. (B) Semantic similarity analysis on Gene Ontology terms enriched in up-regulated genes in hom vs wt comparison (FDR < 0.05) with macro-categories identified using Revigo webtool. (C) Heatmap reporting log2 ratios of observed over expected number of genes (coloured bar) in the intersections between up-regulated genes in Lmna Δ8-11 -/- mice in Pparγ-related GO terms and the bivalent genes identified as above. Fisher's Exact Test p-value = 6.73e-06. wt= Lmna Δ8-11 +/+; hom= Lmna Δ8-11 -/-.
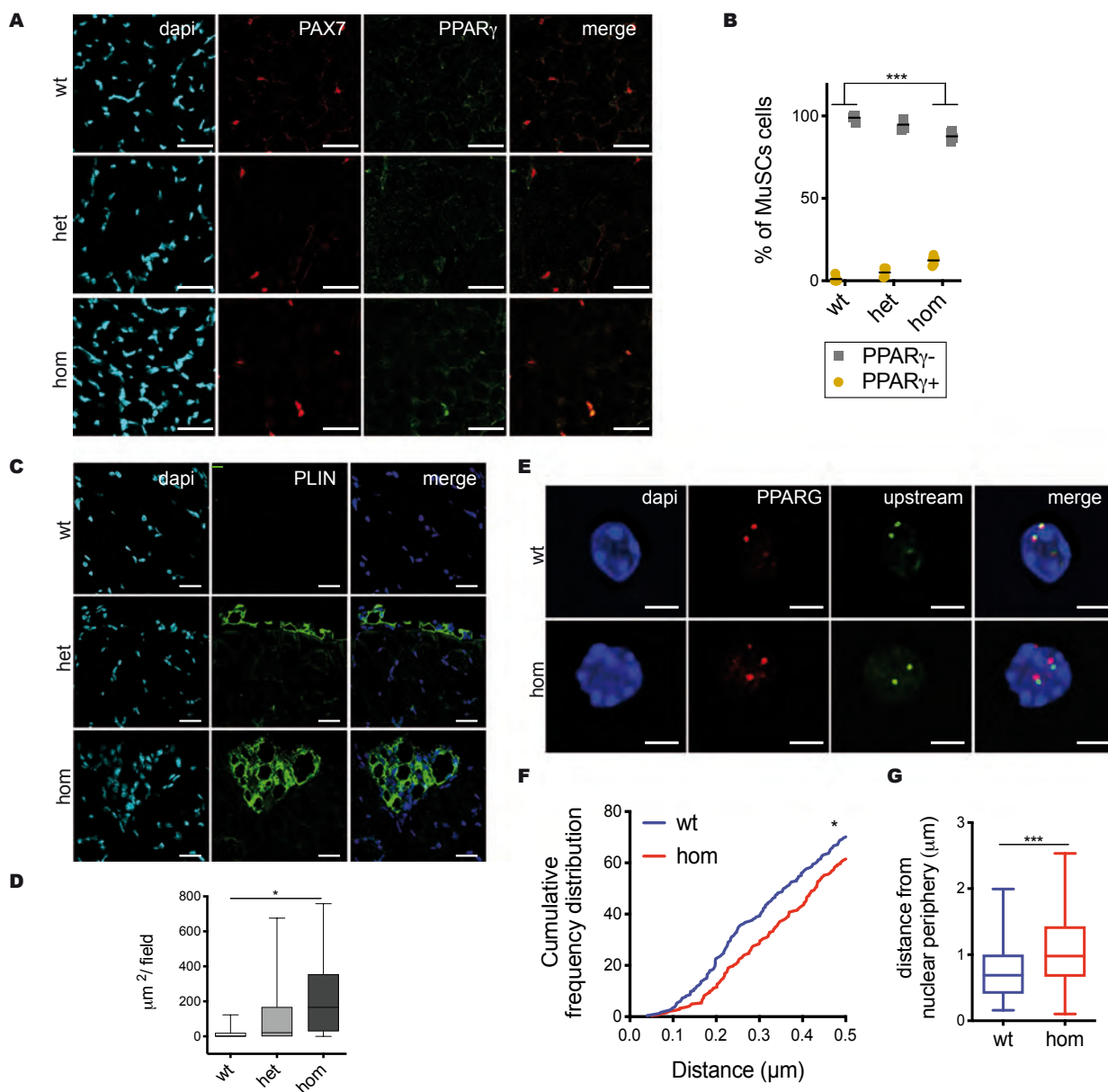
Figure 5. Deregulation of Pparγ locus in Lmna Δ8-11 -/- MuSCs.

(A) Immunohistochemical staining in Lmna Δ8-11 mice of PAX7 and PPARγ markers at 19 days of post-natal growth. Scale bars, 50 μm. (B) Quantification of PPARγ+ MuSCs in (A); n= 4-5 animals per genotype. (C) Immunohistochemical staining in Lmna Δ8-11 muscles of Peripilin at 19 days of post-natal growth. Nuclei of muscle fibers were stained with dapi. Scale bars, 25 μm. (D) Quantification of Peripilin staining in (C); n= 5 animals per genotype. (E) Representative image of FISH analysis of fixed and sorted MuSCs from Lmna Δ8-11 mice at d19 with probes indicated in Supplementary Figure 10. Scale bars, 2 μm. (F) Quantification of FISH probes (represented in Figure S10) distances (x-axis) by cumulative frequency distributions (y-axis). Only probes with distance ≤ 0.5μm are reported. n= 1-2 animals per genotype. (G) Quantification of FISH probes positioning with respect to the nuclear envelope. B, Data are mean ± s.e.m. D, G, Data are box with median and whiskers min to max. B, D, Statistics by two-way analysis of variance (ANOVA) with multiple comparisons. F, G, Comparisons by Kolmogorov-Smirnov test.
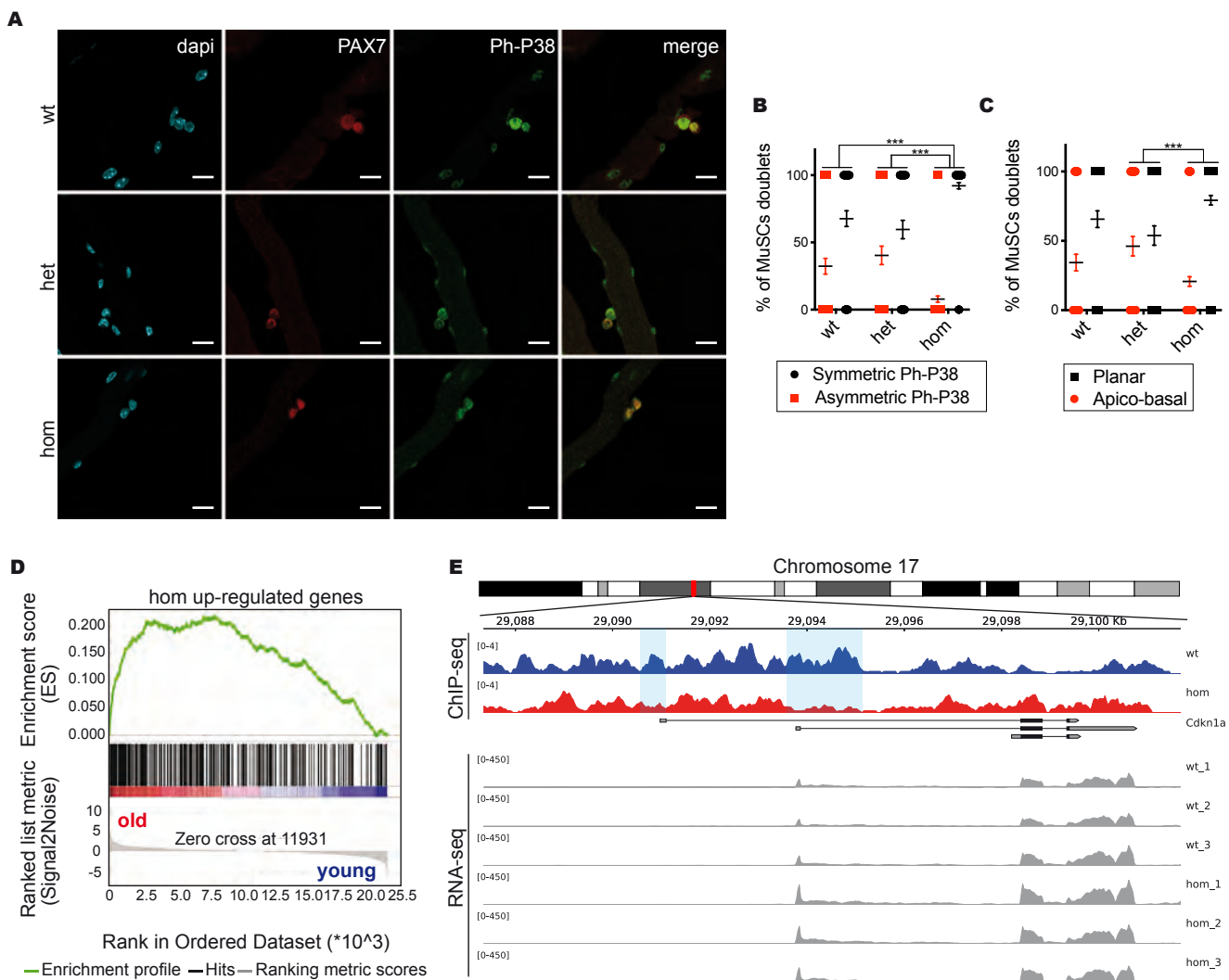* P < 0.05, * * * P < 0.001; wt= Lmna Δ8-11 +/+; het= Lmna Δ8-11 +/-; hom= Lmna Δ8-11 -/-.

Figure 6. Lmna Δ8-11 -/- MuSCs acquire senescence transcriptional traits.

(A) Representative image of myofibers-derived MuSCs from Lmna Δ8-11 mice at d19 immunostained for Ph-P38 and PAX7 after 48 h of culture. Scale bars, 25 µm. (B) Quantification of asymmetric and symmetric divisions assessed by Ph-P38 distribution as shown in (A). (C) Quantification of asymmetric apico-basal division vs symmetric planar divisions. n=46± 6 doublets of MuSCs per genotype, n= 7-9 mice per group. (D) GSEA on expression data from old and young mice quiescent satellite cells (25). Up-regulated (log Fold Change – logFC > 1) genes in hom vs wt comparison added to Biocarta mouse pathways from gskb R package were used as gene sets (NES = 4.70, FDR < 10e-4). (E) ChIP-seq of H3K27me3 mark and RNA-seq signal tracks on Cdkn1a/p21 locus. Promoter regions are highlighted by light blue rectangles. B, C, Data are mean ± s.e.m. Statistics by two-way analysis of variance (ANOVA) with multiple comparisons.
* * P < 0.01; * * * P < 0.001. wt= Lmna Δ8-11 +/+; het= Lmna Δ8-11 +/-; hom= Lmna Δ8-11 -/-.

: QSCs (PAX7+/MYOD-) : ASCs (PAX7+/MYOD+)
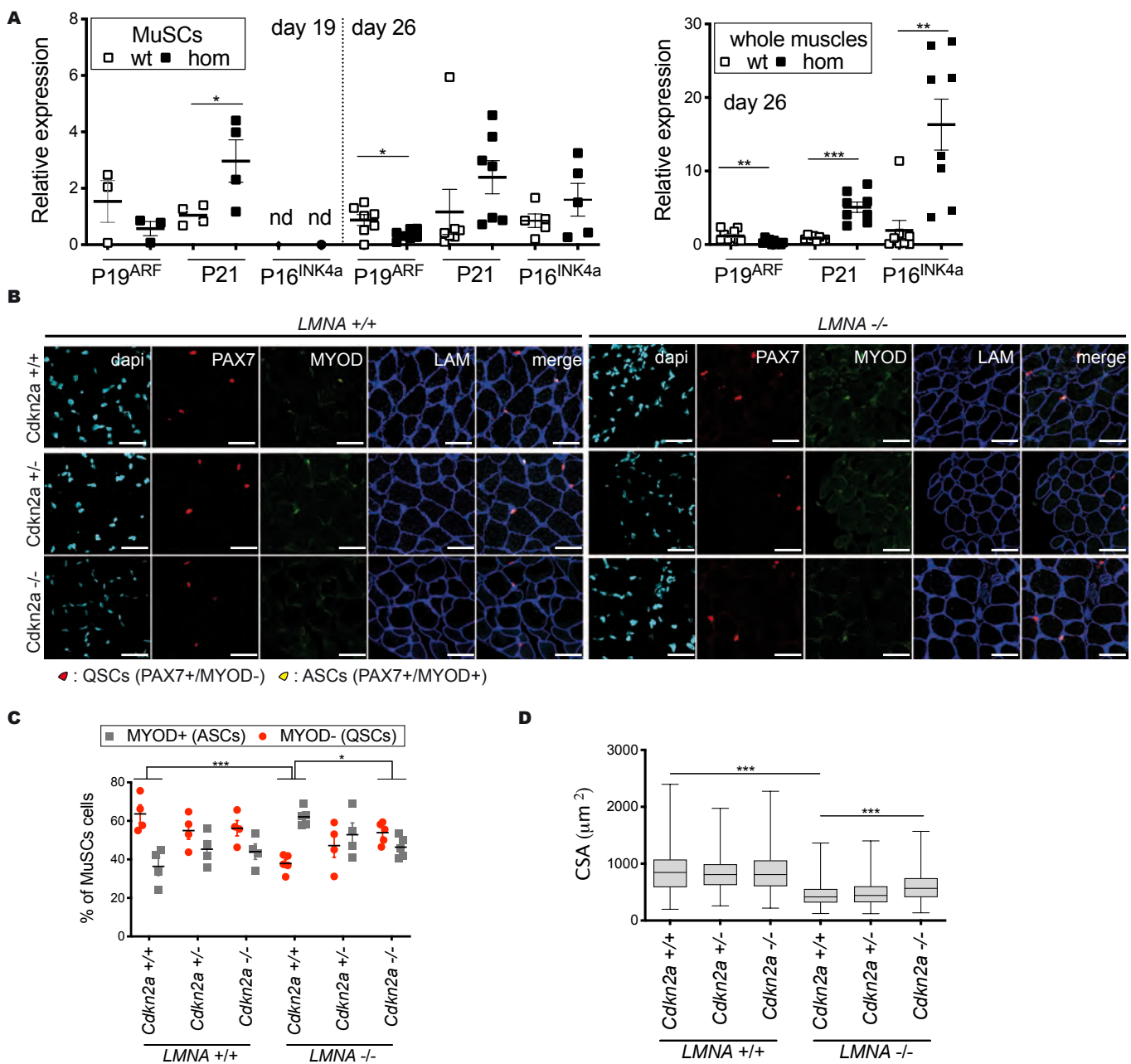
Figure 7. Cdkn2a genetic ablation restores regenerative capacity of Lmna Δ8-11 -/- dystrophic mice.

(A) Transcriptional analysis of p16INK4 and p19ARF at Cdkn2a locus in Lmna Δ8-11 mice MuSCs (left graph) at d19 and d26 days and whole muscles (right graph) at d26 days of postnatal growth. Value were normalized on gapdh and compared with the average of wt amplification. Nd: not detected. n= 3-10 animals per genotype. (B) Immunohistochemical staining in Cdkn2a/Lmna Δ8-11 mice of PAX7 and MYOD markers at d19. Basement membrane of muscle fibers was stained with Laminin. Activated, ASCs (PAX7+/MYOD+) and self-renewing, QSCs (PAX7+/MYOD-) MuSCs are shown. Scale bars, 50 μm. (C) Quantification of MuSCs pool composition in (B). n=4-5 animals per genotype. (D) Quantification of myofibre size, evaluated by the Cross Sectional area (CSA). n= 600 muscle fibers. n=4-5 animals per genotype. A, C, Data are mean ± s.e.m. D, Data are box with median and whiskers min to max. A, Comparisons by unpaired t-test. C, D, Statistics by one-way (D) or two-way (C) analysis of variance (ANOVA) with multiple comparisons.
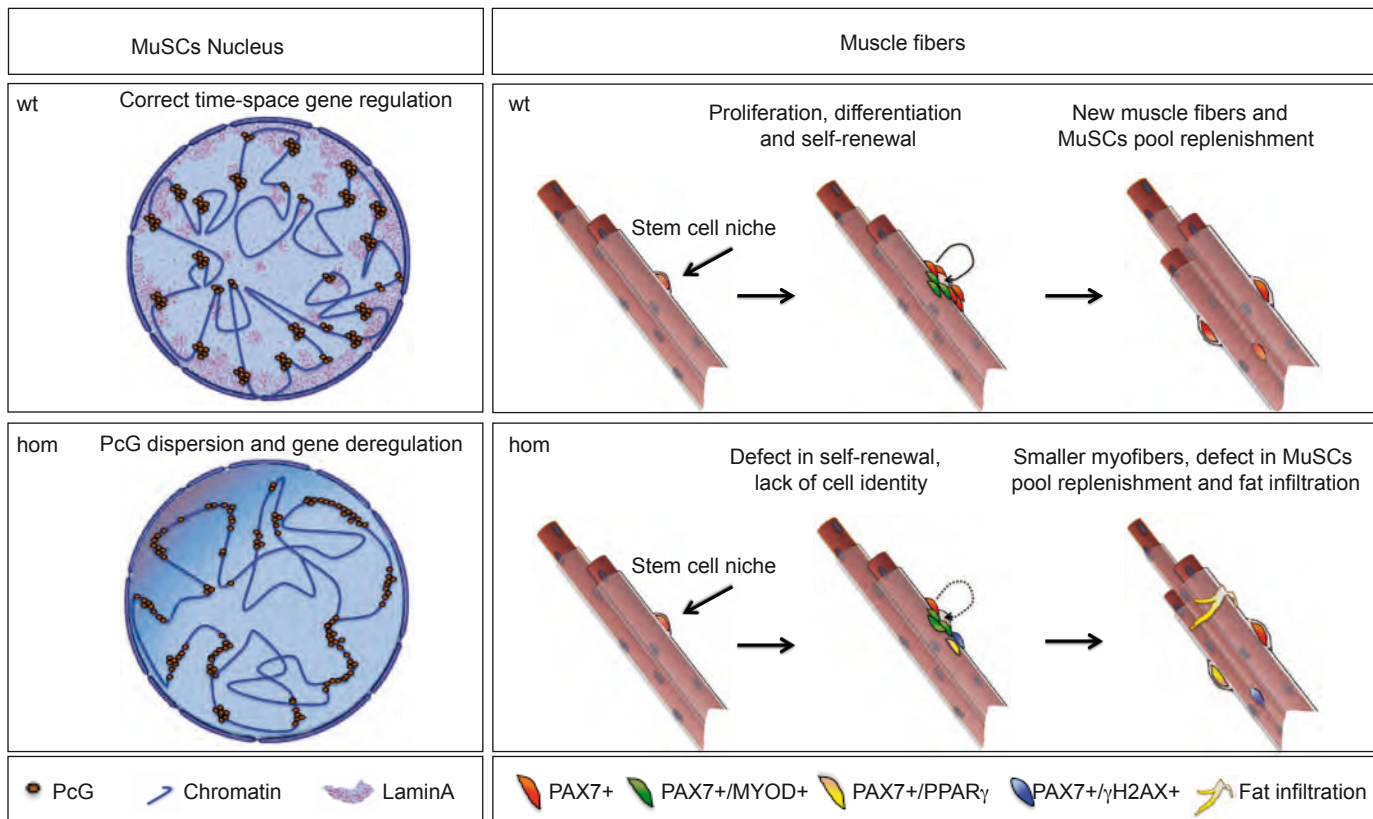* P < 0.05, * * P < 0.01, * * * P < 0.001; wt= Lmna Δ8-11 +/+; hom= Lmna Δ8-11 -/-.

Figure 8. Lamin A/C-Polycomb crosstalk in Lamin dependent muscular dystrophy.

In wt MuSCs the Lamin A/PcG interplay sustains the chromatin higher order structure at differentiation loci, ensuring proper spatio-temporal gene regulation during muscle differentiation. The absence of Lamin A/C determines PcG displacement and relaxation of PcG-mediated higher-order chromatin structure. In Lmna Δ8-11 -/- MuSCs Lamin A/PcG dysfunctional crosstalk causes a lack of cellular identity and premature senescence finally leading to an exhaustion of the stem cell niche and infiltration of adipogenic cells. wt= Lmna Δ8-11 +/+; hom= Lmna Δ8-11 -/-.